Dynamic Mapping of Inland Freshwater Aquaculture Areas in Jianghan Plain, China

Yifei Han, Jinliang Huang, Feng Ling, Juan Qiu, Zhixuan Liu, Xiaodong Li, Cun Chang, and Hong Chi

***Abstract*—Freshwater aquaculture in Jianghan Plain plays a key role in the whole industry of China. It was expanding rapidly to meet the fast-growing demand of consumption in these decades. The spatial distribution change of aquaculture in Jianghan Plain has attracted many researchers in recent years and it is worth further investigating. However, the accuracy and the quality of inland aquaculture classification and mapping still have space to be improved. Our study attempts to use Sentinel-1 and Sentinel-2 data to classify aquaculture areas, nonaquaculture water, and nonwater areas. We applied image segmentation and pixel-based feature computation to obtain candidate datasets. Recursive feature elimination (RFE) was used to find the optimal datasets which were then imported into a modified UNet for classification. This workflow was then applied to the annual datasets for better observation of the spatial change of aquaculture areas. In total, 12 indices and features were found most influential and preserved after RFE. The overall classification accuracy reached 96.83%, while the precision and recall of aquaculture areas reached 84.47% and 90.48%, respectively. The combination of object-based and pixel-based image analysis showed its advantage in inland aquaculture classification compared to other studies. Integrated rice–crawfish farming was found a key factor motivating the rapid development of aquaculture. Policies about the fishing ban and ecosystem restoration were also found deeply affecting the spatial change of aquaculture in Jianghan Plain.**

***Index Terms*—Aquaculture classification, Jianghan plain, recursive feature elimination (RFE), sentinel-1, sentinel-2, spatial change, UNet.**

Manuscript received 19 July 2022; revised 30 November 2022; accepted 17 April 2023. Date of publication 24 April 2023; date of current version 15 May 2023. This work was supported in part by the Joint Funds of the National Natural Science Foundation of China under Grant U22A20567, in part by a grant from the State Key Laboratory of Resources and Environmental Information System, in part by a grant from the State Key Laboratory of Desert and Oasis Ecology, Xinjiang Institute of Ecology and Geography, Chinese Academy of Sciences, in part by a grant from Hubei Provincial Natural Science Foundation for Innovation Groups under Grant 2019CFA019, and in part by the National Natural Science Foundation of China under Grant 62071457. *(Corresponding author: Hong Chi.)*

Yifei Han is with the Key Laboratory of Monitoring and Estimate for Environment and Disaster of Hubei Province, Innovation Academy for Precision Measurement Science and Technology, Chinese Academy of Sciences, Wuhan 430071, China, and also with the University of Chinese Academy of Sciences, Beijing 100049, China (e-mail: hanyifei21@mails.ucas.ac.cn).

Jinliang Huang, Feng Ling, Juan Qiu, and Xiaodong Li are with the Key Laboratory of Monitoring and Estimate for Environment and Disaster of Hubei Province, Innovation Academy for Precision Measurement Science and Technology, Chinese Academy of Sciences, Wuhan 430071, China (e-mail: hjl@apm.ac.cn; lingf@whigg.ac.cn; qiujuan@apm.ac.cn; lixiaodong@apm.ac.cn).

Zhixuan Liu is with the Faculty of Resources and Environmental Science, Hubei University, Wuhan 430062, China (e-mail: 201931108010027@stu.hubu.edu.cn).

Cun Chang is with the State Key Laboratory of Desert and Oasis Ecology, Xinjiang Institute of Ecology and Geography, Chinese Academy of Sciences, Urumqi 830011, China (e-mail: changcun@ms.xjb.ac.cn).

Hong Chi is with the Key Laboratory of Monitoring and Estimate for Environment and Disaster of Hubei Province, Innovation Academy for Precision Measurement Science and Technology, Chinese Academy of Sciences, Wuhan 430071, China, with the State Key Laboratory of Desert and Oasis Ecology, Xinjiang Institute of Ecology and Geography, Chinese Academy of Sciences, Urumqi 830011, China, and also with the State Key Laboratory of Resources and Environmental Information System, Institute of Geographic Sciences and Natural Resources Research, Chinese Academy of Sciences, Beijing 100101, China (e-mail: chihong@whigg.ac.cn).

Digital Object Identifier 10.1109/JSTARS.2023.3269430

I. Introduction

AQUACULTURE is currently a fast-growing food industry and contributes to about 50% of worldwide fish consumption [1]. Dynamic mapping and area change detection have great potential for better understanding the development of the aquaculture industry. In recent years, remote sensing (RS) was found at low cost and highly efficient in achieving such a goal and it has been implemented in many related worldwide studies [2]. In China, many lakes have been reformed into aquaculture areas to meet the increasing food demands these years [3]. Jianghan Plain, where the Yangtze River and Han River cross, is an important region for the freshwater aquaculture industry in China [4]. It has experienced great changes in recent years due to complex social and environmental factors. For example, various wild species such as Chinese paddlefish suffered extermination in the Yangtze River [5]. The Chinese government, therefore, issued a series of fishing ban policies [6] which drove great changes in the aquaculture distribution pattern in Jianghan Plain. The conversion from natural lakes to aquaculture areas caused biodiversity loss in wetlands [7]. The expansion of cage culture in reservoirs and lakes also increased nutrients and thus induced eutrophication [8]. To deal with these serious problems, the officials took many actions such as the demolition of enclosure fences [9]. The dynamic mapping of aquaculture areas in Jianghan Plain was believed important in supervising the policy implementation and guiding the development of the local inland aquaculture industry.

In recent decades, optical satellite images especially multispectral images such as GaoFen-2 [10], Landsat 8 [11], and Sentinel-2 images [2] have been widely used in aquaculture mapping. Synthetic aperture radar (SAR) image such as Sentinel-1 is another RS data type that has been applied to aquaculture classification [12], [13]. The combination of optical images and SAR data was regarded as a better way to classify aquaculture areas. The multispectral information was used to exclude false

positives and thus enhance SAR performance in related studies [1]. However, there was a lack of studies that combined these two RS data to achieve accurate detection of all aquaculture areas on a regional scale. Most studies focused on small-area aquaculture extraction or enclosure fence classification [9].

Currently, pixel-based image analysis (PBIA) and object-based image analysis (OBIA) are two popular methods to help extract aquaculture areas from satellite images. PBIA methods such as convolutional neural networks (CNN) and semantic segmentation have been confirmed useful in aquaculture classification studies. For example, Fu et al. [14] designed a CNN-based method to classify marine aquaculture areas. Cui et al. [15] used a fully convolutional network (FCN) to achieve pixel-level categorization of floating raft aquaculture. OBIA segments the image into objects composed of mutually related pixels and thus utilizes more abundant features than PBIA [16]. Ren et al. [17] took the image segmentation method and identified the aquaculture ponds by Normalized Difference Water Index (NDWI). Liu et al. [18] combined object-oriented NDWI and edge features to extract raft and cage aquaculture areas. Xu et al. [2] imported multiple object indices such as Normalized Difference Vegetation Index (NDVI) into a random forest (RF) classifier to generate the aquaculture map. However, the pixels which belong to the same category may not have identical spectral features and this would cause poor PBIA quality. Purely using OBIA may also be inappropriate considering that the multiscale segmentation is not perfect when the adjacent pixels which belong to different classes have similar spectral properties. The classification accuracy might get worse when there exist mixed pixels. The combination of PBIA and OBIA is important to utilize the advantages of both methods.

Although many studies focused on the classification of aquaculture areas, most of these researches were about marine aquaculture ponds or raft aquaculture instead of inland aquaculture areas. Compared to marine aquaculture, inland aquaculture comprises many different categories such as scattered small aquaculture ponds among arable lands and integrated rice–crawfish (IRC) farming areas. Some scholars such as Zeng et al. [19] designed an algorithm to extract aquaculture ponds around inland lakes on medium-resolution multispectral images. However, in Jianghan Plain, many ponds are scattered around the arable lands and some of these waters are small reservoirs or farm ponds used for irrigation rather than intensive aquaculture (see Fig. 1). A more suitable inland freshwater aquaculture classification method is needed.

In this study, we aimed at exploring the optimal classification solution for Jianghan Plain aquaculture areas and analyzing its spatial changes in three major steps.

1) Pixel and object-based datasets from Sentinel-1 and Sentinel-2 images were produced and used to find the optimal datasets influencing classification.

2) Based on the selected datasets, we trained a modified deep-learning classification model and compared it with other existing methods.

3) We applied our classification method to achieve dynamic mapping and observation of spatial change.

Fig. 1. Typical ponds in Jianghan plain. (a) Reservoir and ponds for irrigation. (b) Small area intensive aquaculture ponds scattered around arable lands.

II. Materials and Methods

A. Study Area

Jianghan Plain is located in the middle-south of Hubei Province, China. The Yangtze River and Han River float across and converge on this plain which encompasses about an area of 40000 km^2 [20]. In this study, we picked 16 counties in Jianghan Plain (29°25′–31°09′N and 111°14′–114°06′E) as our study area (see Fig. 2). These counties covered the most important intensive aquaculture areas of Jianghan Plain such as Honghu Lake.

B. Raw Datasets

In this study, the SAR data we used were Sentinel-1A images captured from Alaska Satellite Facility Distributed Active Archive Center.[1] We used both vertical-horizontal (VH) and vertical-vertical (VV) polarized SAR data in interferometric wide-swath mode and the ground range detected high-resolution format. We selected four scenes of Sentinel-1 images that covered the whole study area and they were all captured closest to December 1st each year considering that the aquaculture areas were less likely to be flooded by the lake in the dry season (see Fig. 3). Also, the average monthly precipitation of a typical prefecture in Jianghan Plain, Jingzhou, reached the lowest in

[1] [Online]. Available: https://asf.alaska.edu/

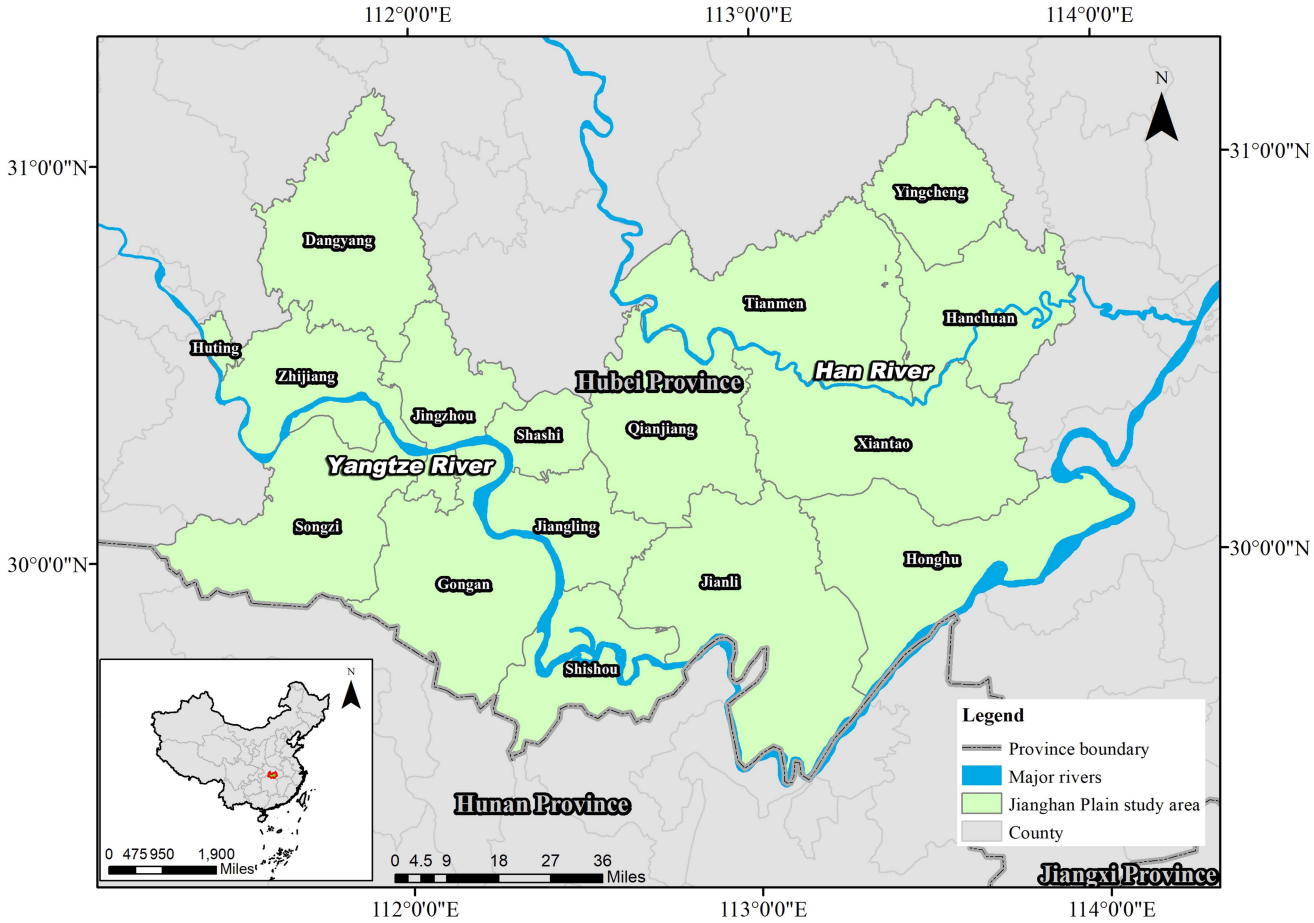

Fig. 2. Geographic location of Jianghan plain.

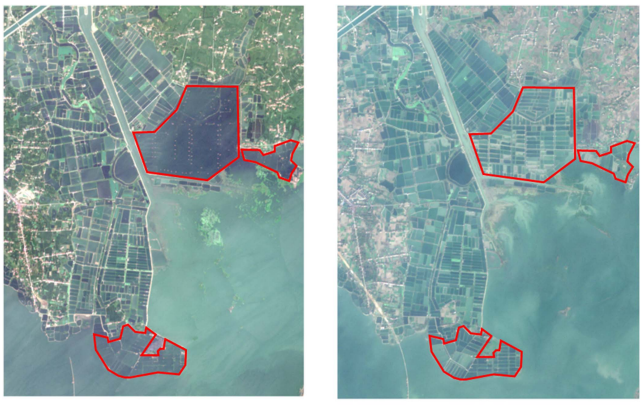

Fig. 3. Aquaculture areas around Changhu Lake on (a) August 1, 2016 and (b) December 9, 2016. Flooded aquaculture areas were outlined in red.

December (0.6 inches). In total, 24 scenes from 2016 to 2021 were obtained.

The optical data we used was Sentinel-2 Level-1C (L1C) Top-Of-Atmosphere products downloaded from U.S. Geological Survey website.[2] Jianghan Plain was covered by eight scenes of Sentinel-2 images and we used a total of 48 images for the mapping from 2016 to 2021. All scenes of Sentinel-2 images were also captured at the date closest to December 1st.

[2][Online]. Available: https://earthexplorer.usgs.gov/

C. Methodology

The workflow of our study is shown in Fig. 4 and explained in detail thereafter. Our work consisted of five parts: data preprocessing, index and feature computation, optimal datasets selection, classification, and spatial change observation.

1) Data Preprocessing: All these Sentinel-1 SAR images were then preprocessed using the method introduced in [21] to generate 10 × 10 m spatial resolution images which represented VV and VH polarization measurements. We applied Sen2Cor v2.9 to accomplish the preprocesses including applying orbit files, thermal noise and border noise removal, calibration, speckle filtering, terrain correction, and conversion to dB.

Sen2Cor was also applied to correct the effects of the atmosphere, and thus we produced Level-2A (L2A) corrected reflectance images as introduced in [22]. We selected widely-used six bands from these L2A images in our study (see Table I).

2) Index and Feature Computation: In this study, we calculated many types of indices based on preprocessed Sentinel-1 and Sentinel-2 data as the import.

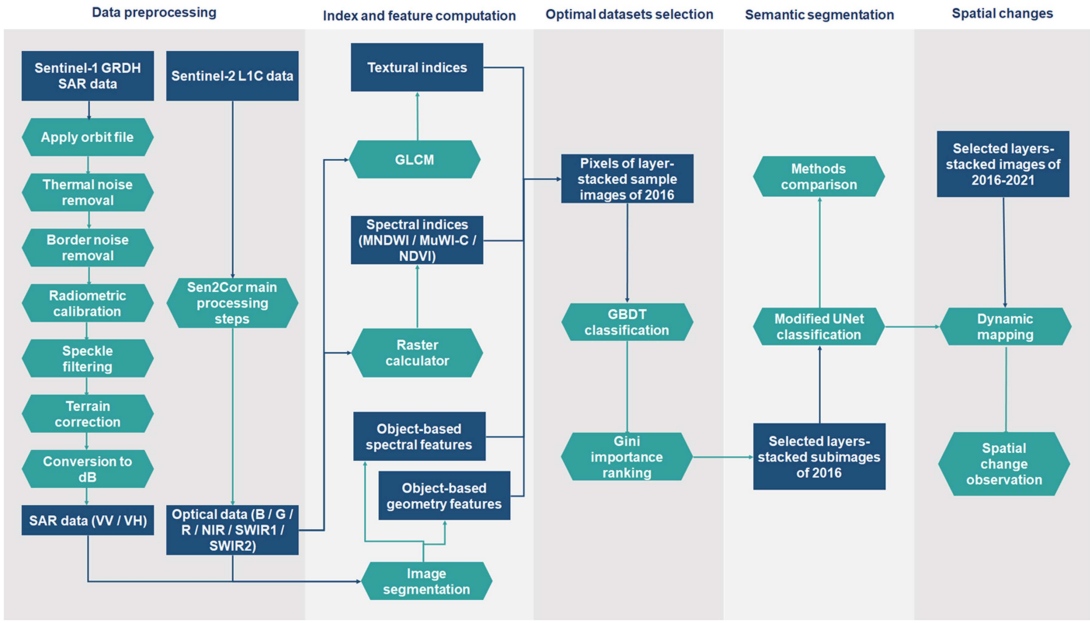

Fig. 4. Overall workflow of our study.

TABLE I
BANDS SELECTED FROM SENTINEL-2 L2A DATA

Band type	Central wavelength (nm)
Blue	490
Green	560
Red	665
Near-infrared	842
Short-wave infrared	1610

Three spectral indices calculated based on band information from Sentinel-2 images were applied to help extract aquaculture ponds: Modified Normalized Difference Water Index (MNDWI), Complete version of Multi-Spectral Water Index (MuWI-C), and NDVI. MNDWI and MuWI-C were proven reliable in water mapping on Sentinel-2 and we used the calculation method introduced in [23] and [24] to produce the maps. NDVI was another widely-accepted index effective in aquaculture area recognition considering that aquaculture areas usually have higher nutrients and higher algae concentrations compared to natural water bodies [2]. We did not use NDWI in our study because MNDWI was found more accurate in water body extraction than NDWI [23]. These three spectral indices were calculated by the following equations:

$$\mathrm{NDVI} = (NIR - R)/(NIR + R) \tag{1}$$

$$\mathrm{MNDWI} = (G - SWIR1)\,/\,(G + SWIR1) \tag{2}$$

$$\begin{aligned}\mathrm{MuWI-C} &= -16.4ND\,(B,G) - 6.9ND\,(B,R)\\ &\quad -8.2ND\,(B,NIR) - 8.8ND\,(B,SWIR1)\\ &\quad +9.6ND\,(B,SWIR2) + 10.8ND\,(G,NIR)\\ &\quad +6.1ND\,(G,SWIR1) + 13.6ND\,(G,SWIR2)\\ &\quad -0.28ND\,(R,NIR) - 3.9ND\,(R,SWIR1)\\ &\quad -2.1ND\,(R,SWIR2) - 5.3ND\,(NIR,SWIR1)\\ &\quad -5.3ND\,(NIR,SWIR2) - 5.3ND\,(SWIR1,SWIR2)\\ &\quad -0.33\end{aligned} \tag{3}$$

where *B*, *G*, *R*, *NIR*, *SWIR*1, and *SWIR*2 are the optical bands of Sentinel-2 images. *ND(i, j)* represents the normalized difference between Sentinel-2 band *i* and band *j*.

Grey-level Co-occurrence Matrix (GLCM) was the most commonly used method to extract texture information from images [25], and it was proved useful in aquaculture area classification [10], [14]. In this study, we first used principal components analysis [26] to generate the first few principal component layers which indicated over 99% of the information of the input Sentinel-2 images. Then we applied the GLCM of 5 × 5 kernel size to the preserved principal components and extracted seven textural indices including angular second moment, contrast, dissimilarity, energy, entropy, homogeneity, and stand deviation (Std).

All selected Sentinel-2 bands as well as Sentinel-1 VV and VH images were stacked in ArcMap 10.8 and were then imported into the software eCognition v9.0 for segmentation and object feature extraction. The segmentation method we used was the multiresolution algorithm [27]. We tested different scale parameters (*S*), shape/color parameters (w_{sha}/w_{col}), and compactness/smoothness parameters (w_{com}/w_{smo}) multiple times and set them to 20, 0.5, and 0.8, respectively, to ensure that most aquaculture ponds were distinguished from the background and they were intact enough.

TABLE II
DETAILS OF ALL 33 LAYERS USED IN THIS STUDY

Layer Type	Layer description
SAR data	VV, VH[a]
Optical data	B, G, R, NIR, SWIR1, SWIR2[b]
Spectral indices	MNDWI, MuWI-C, NDVI[c]
Textural indices	Angular second moment, Contrast, Dissimilarity, Energy, Entropy, Homogeneity, Standard deviation
Object-based spectral features	Standard deviation of layer i (i = B, G, R, NIR, SWIR1, SWIR2, VV, VH),
Object-based geometry features	Area, Compactness, Density, Elliptic fit, Length-width ratio, Rectangular fit, Shape index

[a] VV: Vertical-Vertical polarization; VH: Vertical-Horizontal polarization.
[b] B: Blue; G: Green; R: Red; NIR: Near infrared; SWIR: Short wave infrared;.
[c] MNDWI: Modified Normalized Difference Water Index; MuWI-C: Complete version of Multi-Spectral Water Index; NDVI: Normalized Difference Vegetation Index.

The object-based features which we captured from the segmented object layers were two types: spectral features and geometry features. The spectral features we obtained were the standard deviations of each object on different layers. The geometry features included area, compactness, density, elliptic fit, length-width ratio, rectangular fit, and shape index (SI). The calculation and explanation of these features can be found in [28], [29], and [30].

All the data used in this study were listed in Table II and they were converted to band layer format as the input for the following procedures. The object-based features were also transferred to layer format where the feature value of each object was inherited by each pixel in the extent of this object.

3) Optimal Datasets Selection: Considering that in total 33 layers were stacked as the input for each scene, it was necessary to reduce the dimension to ease the computation load. Also, high-dimensional data might include layers that were not helpful enough in learning the features of aquaculture areas and this would cause an overfitting problem [31].

Recursive feature elimination (RFE) is an algorithm used to find the optimum number of features performing well in the analysis [32]. In this study, we applied RFE to filter out the redundant layers considering that it was also proved effective in OBIA [33].

In our study, we used Python 3.8.8 with the package Scikit-learn 0.24.2 to build a Gradient Boosting Decision Tree (GBDT) based classification model to conduct RFE. Similar to the popular RF algorithm, GBDT is also in the form of ensemble decision trees but usually performs better than RF does [34]. The Gini index which represents the importance of each parameter can be calculated by the following equation [35]:

$$G_k = 2p(1-p) \tag{4}$$

where G_k is the Gini index of node k, and p is the fraction of the positive example assigned.

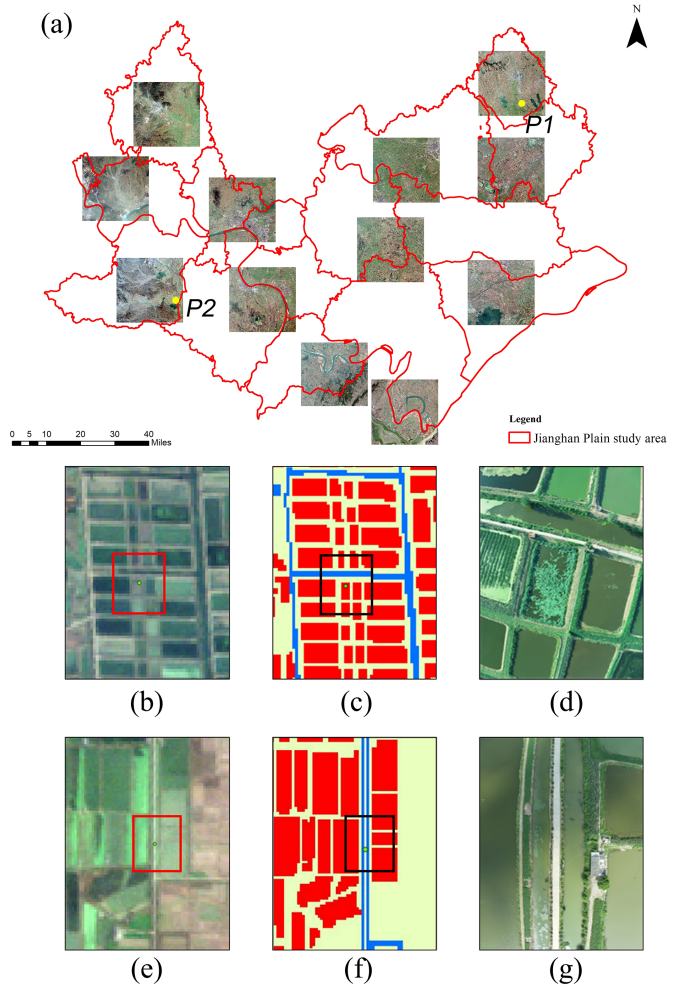

Fig. 5. Extents of sample images and manually labeled images. (a) Presents the extent of 12 sample images (true color) cropped out from the all-layer-stacked images of December 9, 2016. (b)–(d) True color image, the manually labeled image, and the UAV-based field survey photo of point P1. (e)–(g) Present the true color image, the manually labeled image, and the UAV-based field survey photo of point P2.

We cropped 12 sample images out of all-layer-stacked full images of 2016. The extent of each sample image was about 3100 × 3100 pixels (see Fig. 5). All these 12 sample images were manually classified into three categories: aquaculture areas (AA), non-aquaculture water (NA), and nonwater areas (NW). AA and NA are both water-based. To help understand their differences, we present some typical images of both these two categories in Fig. 6. We selected several areas to take field surveys and then manually labeled all sample images. Some areas were verified by the field survey results (see Fig. 5). We did a field survey by using an unmanned aerial vehicle (UAV) to capture the photos which matched the selected areas on satellite images. After manual labeling, we exported the values of 33 layers for each pixel and randomly selected one million pixels as the input for the GBDT model.

According to RFE, we removed the parameter with the lowest Gini index after we trained the GBDT classification model for each time until the classification accuracies continuously decreased for three iterations and the latest accuracy was lower

Fig. 6. Typical aquaculture areas and nonaquaculture water areas in Jianghan plain.

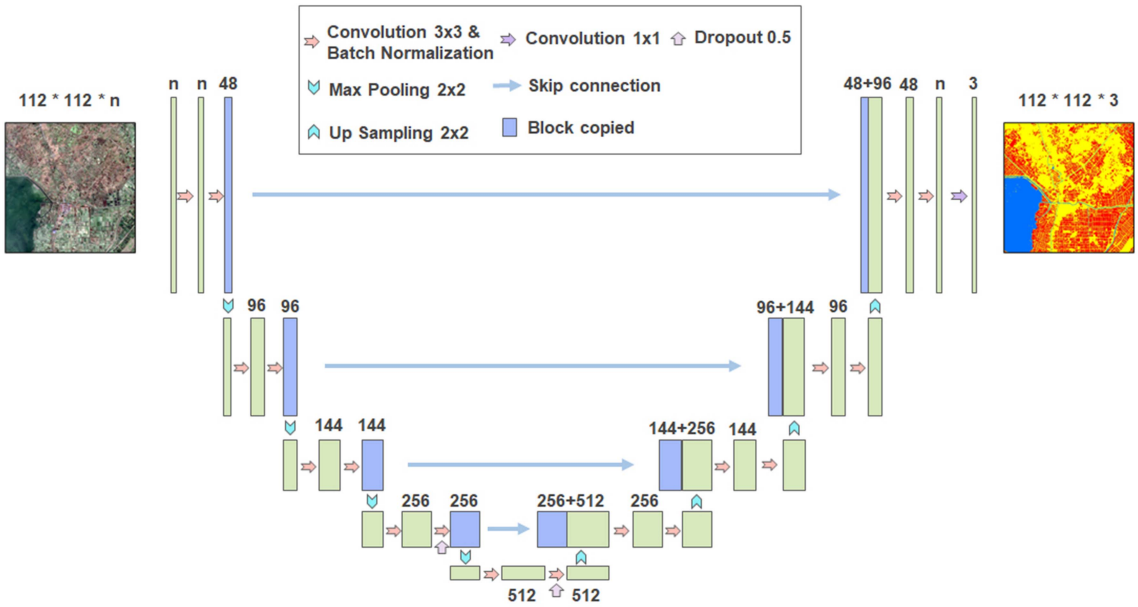

Fig. 7. Modified UNet architecture used to classify aquaculture areas.

than 95%. This rule ensured that the dimension of the retained layers can be as small as possible while most useful parameters can be preserved.

4) Aquaculture Area Classification and Spatial Change Observation: The pixel-based image classification method we used in this study was deep learning-based semantic segmentation developed in recent years. Semantic segmentation usually outperformed traditional pixel-based classification methods such as maximum likelihood [36]. We constructed a modified UNet (see Fig. 7) to achieve highly accurate recognition of the aquaculture area. UNet is a form of FCN and it has been proven effective in different land use and land cover tasks [37], [38]. The modified UNet was implemented using Python 3.8.8 with the TensorFlow 2.7.0 framework and trained on NVIDIA 3080 Ti GPU.

We used all 12 sample images but only preserved n layers (n represented the number of layers preserved after RFE). Then we split all sample images into 9630 subimages where the extent of most of them was 112 × 112 pixels. There were still a few marginal subimages smaller than this size. Considering the serious data imbalance problem, we selected 1600 subimages according to the proportion of non-water pixels in each subimage to make sure the pixel numbers of different classes were closer. We picked the first 1600 subimages following the ascending order of nonwater pixel proportion. However, most subimages were dominated by nonwater pixels. To make sure all types of land cover were included in our study, we randomly preserved 100 subimages from the left 8030 subimages where nonwater areas occupied most of the pixels. Therefore, the number of sample subimages finally reached 1700. The modified UNet started with the input of 112 × 112 × n pixel size, the margin subimages were reshaped before training. All these 1700 subimages were randomly split into 1550 training and 150 validation sets. The numbers of sample pixels by each class were presented in Table III.

There are two main differences between our modified UNet and the original UNet [39]. First, our modified UNet was more concise that it only comprised 19 convolutional layers rather than 23 in most popular UNet structures. Second, except for

TABLE III
INFORMATION ON THE TRAINING SETS

Category of labeled pixel	Pixel number	Proportion
Aquaculture areas	3 599 309	19.21%
Non-aquaculture water	5 882 553	31.40%
Non-water areas	9 252 777	49.39%

the last convolutional layer, each layer was followed by a batch normalization layer to accelerate the training speed and also increase the network stability. There were also some small changes compared to the popular UNet architectures and should be noticed. The first 18 convolutional layers all used a 3×3 kernel size because some aquaculture ponds were very small and dense, the larger kernel size might smooth the edge and corner feature delivered to the next layer which made it less efficient to learn the features. There was also a 1×1 convolutional layer inserted before output. All activation functions applied in this architecture were ReLU except the one for the last convolutional layer, which used Softmax. In addition, we inserted two dropout layers (dropout $= 0.5$) before the end of the last two blocks in the encoder to avoid the overfitting problem.

The output of this modified UNet was transformed into a prediction map of three classes (AA, NA, NW). We randomly created 10000 checkpoints in our study area excluding the extent of all 12 sample images, considering the cost of a comprehensive field survey, here we labeled all these checkpoints purely by visual interpretation and manually assessed the classification result by analyzing the confusion matrix and the precision and recall. The precision of class A shows the proportion of correctly classified A pixels in all the pixels recognized to be A by the classifier. Whereas recall represents the number of correctly classified A pixels out of all ground truth class A pixels. The accuracy (ACC), precision (P), and recall (R) were computed by the following equations:

$$\mathrm{ACC} = \frac{\sum_{i=0}^{3} c_i}{3} \tag{5}$$

$$P = c_i / m_i \tag{6}$$

$$R = c_i / n_i \tag{7}$$

where c_i is the number of correct classifications of the ith category, n_i is the number of checkpoints manually labeled the ith category, and m_i is the number of checkpoints predicted to be the ith category. The classification result of our method was then compared with two other existing methods: 1) the object spectral feature-based extraction [17]; and 2) the spectral-spatial-morphological-based extraction method [40].

All full extent n layers-stacked images from 2016 to 2021 were then cropped into subimages and classified via the modified UNet. The classified maps were produced by mosaicking. The changes in the spatial distribution of all aquaculture areas between different years in the Jianghan Plain study area were analyzed by taking the social factors into account.

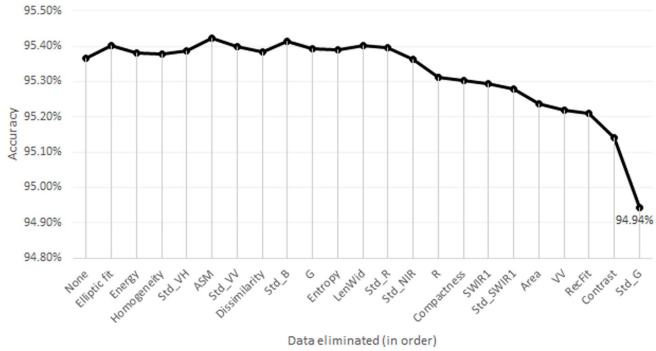

Fig. 8. Data eliminated before each iteration and the corresponding GBDT classification accuracy (None: first iteration without eliminating any data; Std_i: standard deviation of layer i; ASM: angular second moment; LenWid: length/width ratio; RecFit: rectangular fit).

TABLE IV
OPTIMAL DATASETS PRESERVED AFTER RFE

Data preserved	Importance (Gini index)
MuWI-C	0.3666
MNDWI	0.1517
NIR	0.0899
B	0.0757
Density	0.0713
VH	0.0713
SWIR2	0.0428
Shape index	0.0354
NDVI	0.0328
Std	0.0232
Std_SWIR2	0.0198
Std_G	0.0195

III. RESULTS

A. Results of the Optimal Dataset Selection

In total, 21 types of data were found not necessary enough by our RFE results (see Fig. 8). The 22nd iteration presented an accuracy below 95% and the accuracy has been decreasing for over three iterations, therefore the standard deviation of layer G and all the uneliminated data were preserved to be our optimal datasets. Although the accuracy after the 12th iteration kept decreasing, it was still over 95% before the 22nd iteration and such decreasing trend is mild. The tradeoff of taking RFE to reduce dimensions rather than keeping these data was reasonable. All these preserved data as well as their importance (Gini index) were listed in Table IV.

B. Results of Classification by Different Methods

The modified UNet introduced in our study was compared with the methods proposed by the authors in [17] and [40]. Duan et al. [40] used multiple features including MNDWI and Automated Water Extraction Index (AWEI) as thresholds and took a decision tree algorithm to split aquaculture ponds. Ren

Ren's method

Manually labelled category \ Classified category	AA	NA	NW	Recall
AA	564	57	276	62.88%
NA	55	522	43	84.19%
NW	33	18	8432	99.40%
Precision	86.50%	87.44%	96.35%	**Accuracy = 95.18%**

(a)

Duan's method

Manually labelled category \ Classified category	AA	NA	NW	Recall
AA	691	31	175	77.03%
NA	30	549	41	88.55%
NW	73	33	8377	98.75%
Precision	87.03%	89.56%	97.49%	**Accuracy = 96.17%**

(b)

Our method

Manually labelled category \ Classified category	AA	NA	NW	Recall
AA	827	26	61	90.48%
NA	40	537	43	86.61%
NW	112	35	8319	98.26%
Precision	84.47%	89.80%	98.77%	**Accuracy = 96.83%**

(c)

Fig. 9. Confusion matrixes of classification results by (a) REN's method [17]; (b) Duan's method [40]; (c) our method. (AA: aquaculture area; NA: nonaquaculture water; NW: nonwater area).

et al. [17] used rulesets to obtain objects and used the NDWI threshold to filter aquaculture ponds. Ren's method was slightly modified by us applying RF to split AA and NA. All these three methods were tested on the randomly created 10000 checkpoints and their confusion matrixes were presented in Fig. 9.

The confusion matrixes showed that our method outperformed the other two on both AA and NA classifications. It was inspiring that our recall of aquaculture areas classification reached 90.48%. The overall accuracy of our method was also higher than the other two but the gap was not that obvious.

We compared the classification results and selected two small regions as examples which were shown in Figs. 10 and 11.

Fig. 10 showed that our method recognized most of the intensive aquaculture areas near the lake, and the ditch was also correctly categorized as NA rather than AA classified by the other two methods. Ren's method was the least accurate, almost 1/3 of the aquaculture ponds were interpreted as NA. As for the typical AA scattered in arable land (see Fig. 11), we found that our classification method was still the most reliable one. Fig. 11(a) showed that Ren's method ignored many aquaculture ponds. Besides, some nonaquaculture ponds and even the river were misclassified as aquaculture areas by both Ren's and Duan's methods.

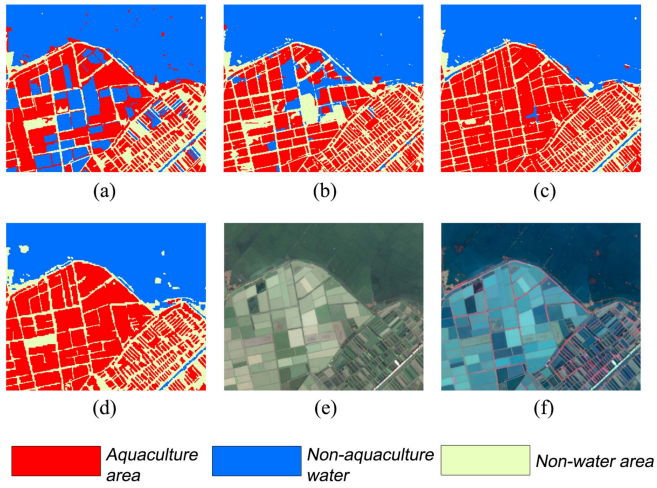

Fig. 10. Classification results of a sample aquaculture area near Honghu Lake by three methods. (a)–(c) Results of Ren's method [17], Duan's method [40], and our method, respectively. (d) Manually labeled map. (e) True color image. (f) False color image (R: NIR; G: red; B: green).

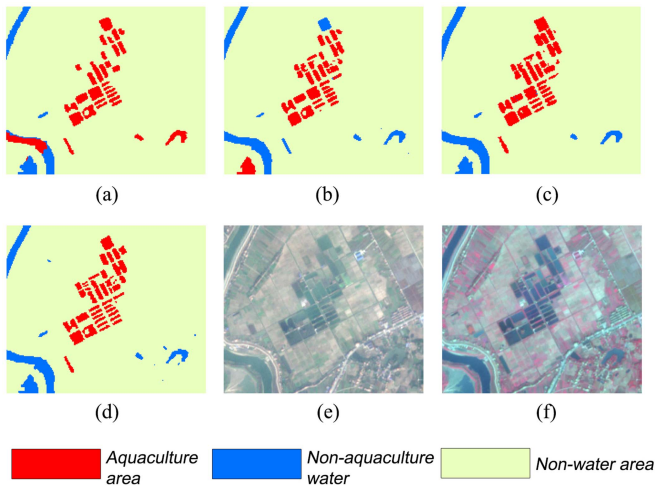

Fig. 11. Classification results of a sample aquaculture area surrounded by arable land by three methods. (a)–(c) Results of Ren's method [17], Duan's method [40], and our method, respectively. (d) Manually labeled map. (e) True color image. (f) False color image (R: NIR; G: red; B: green).

C. Spatial Distribution and Its Change of the Aquaculture in Jianghan Plain

Our method was applied to the images from 2016 to 2021 to better observe the spatial changes in aquaculture areas in Jianghan Plain. The mapping of each year was presented in Fig. 12. It can be seen that most of the aquaculture areas were distributed around Honghu Lake located in the southeast part of Jianghan Plain. Besides, there was also a clear expansion of aquaculture areas in the middle part of Jianghan Plain during these years.

The area change in the aquaculture industry in Jianghan Plain during these years was mapped and recorded (Figs. 13 and 14). We found that the aquaculture area kept expanding and reached the largest in 2019, 2750.18 km^2. This number then suddenly declined to 2224.53 km^2 in 2020 and recovered to 2705.03 km^2

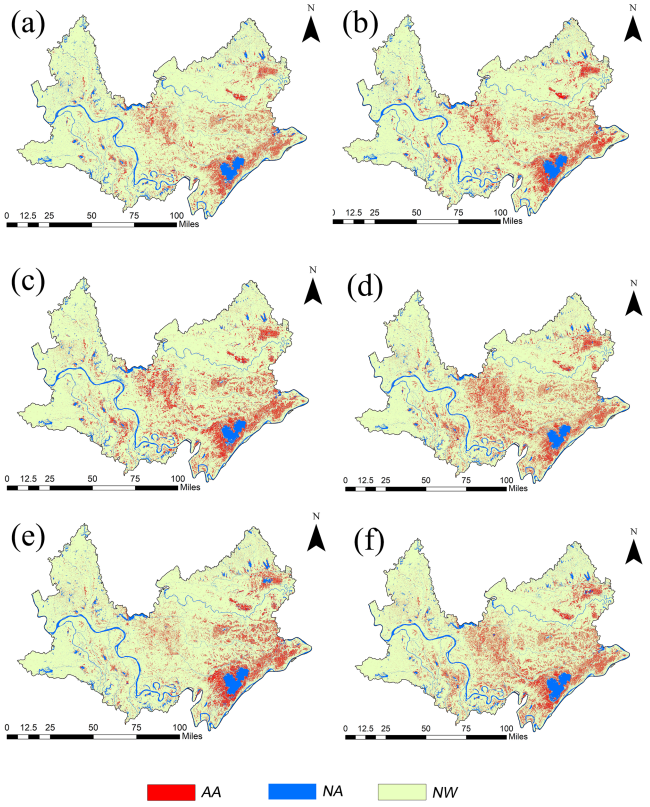

Fig. 12. Annual aquaculture maps of the Jianghan plain study area. (a)–(f) Mapping from 2016 to 2021, respectively.

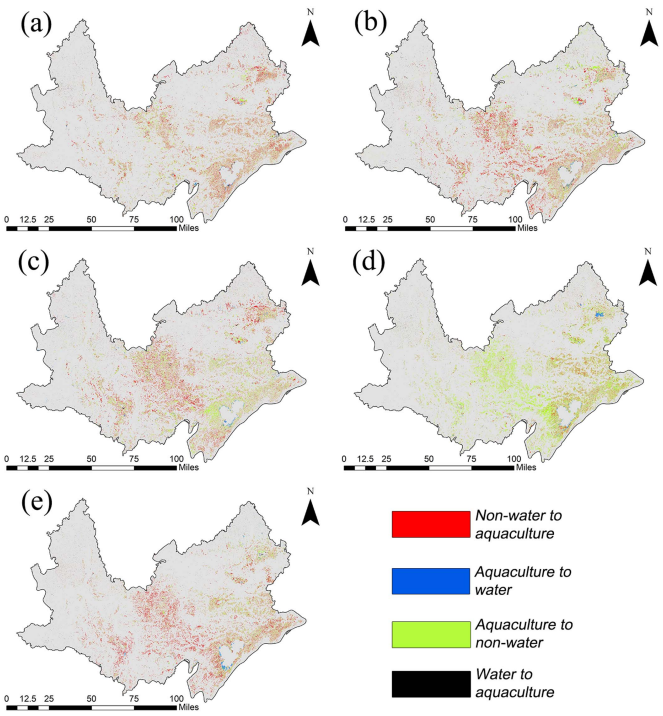

Fig. 13. Aquaculture spatial change maps of the Jianghan plain study area. (a)–(e) Changes from 2016 to 2017, 2017 to 2018, 2018 to 2019, 2019 to 2020, and 2020 to 2021, respectively.

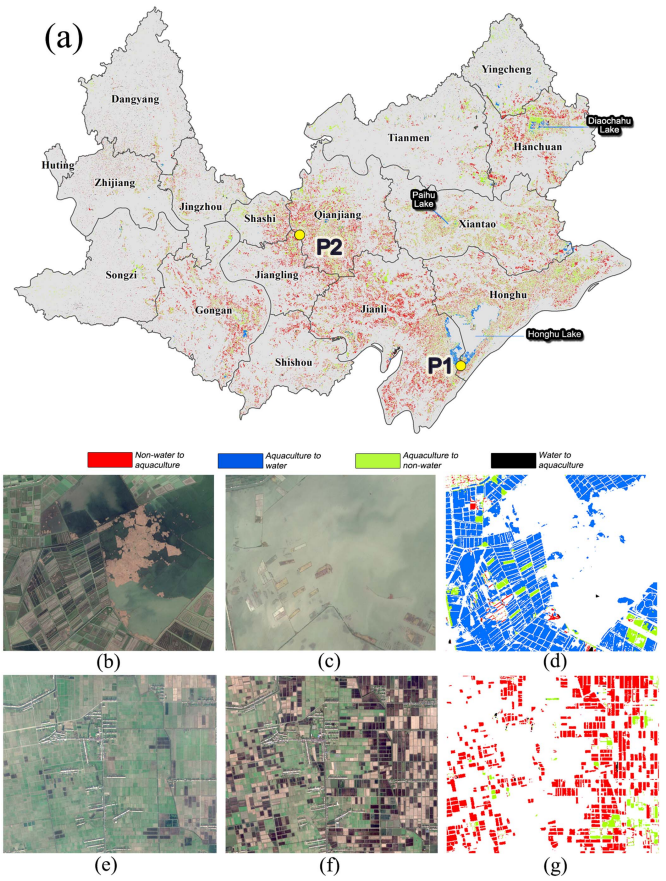

Fig. 14. Aquaculture-related change in Jianghan plain between 2016 and 2021. (a) Typical aquaculture-related area changes. (b)–(d) Image of December 9, 2016, the image of November 18, 2021, and the land class change map of Honghu Lake (P1). (e)–(g) Image of December 9, 2016, the image of November 18, 2021, and the land class change map of Qianjiang county (P2).

in 2021. Besides, we also compared the aquaculture area map of 2016 and the latest map of 2021. Fig. 14 showed that many aquaculture areas in Honghu Lake and Diaochahu Lake located in Hanchuan were reformed into water. The surrounding aquaculture ponds were also removed and changed to nonwater land cover. The expansion of aquaculture areas was also significant, especially in Hanchuan and the middle part of Jianghan Plain. Some typical changes were presented in Fig. 14.

IV. Discussion

A. Analysis of the Datasets Selection

Our feature selection experiment presented interesting results. The two spectral indices, MuWI-C and MNDWI, showed dominant influences. Both these two indices displayed a highly reliable capability in water-related land use extraction. The Gini index of MuWI-C even exceeded 0.3, which means that it is the core factor influencing the classification result.

We also found that most of the optimal datasets preserved were spectral-related. For example, all three spectral indices were found important and some other raw bands such as B, NIR, and SWIR2 were also retained. In addition, object-based

data also showed some contribution to the classification. The SI, density, as well as standard deviation of band G and band SWIR2, were all related to the inspiring classification results. It is worth noticing that the shape of intensive aquaculture areas was usually regular, unlike nonaquaculture water such as reservoirs. The shape of the ditch was also different from most aquaculture ponds as it was usually very narrow and long. These could be vital reasons for explaining the preservation of SI in our optimal datasets. The results of Ren's method and Duan's method also indicated the importance of SI, because both of them existed the wrong classification of rivers and ditches (see Figs. 10 and 11).

The Gini importance of VH was only 0.0713 which means that although the importance of the backscatter feature still exceeded most other datasets, even typical geometry features and textural features, it was still not that significantly contributing to the classification. A possible explanation was that the raw spatial resolution of Sentinel-1 SAR data was not high enough to support the precise classification, the resampled data was still far from the ground truth.

B. Analysis of the Classification Method

Compared to the traditional pixel-based classification methods such as index threshold analysis, the use of modified UNet in our study had the advantage that the suitable convolutional layers helped to learn the spatial pattern [41] especially when our modified UNet was very deep. Our method not only extracted the water from the background but also learned the unique spatial distribution patterns to distinguish the aquaculture area and nonaquaculture water. For example, the isolated reservoir would not be classified as an intensive aquaculture pond and vice versa. In comparison, Ren's and Duan's methods neglected the spatial distribution pattern and their classification results were therefore disrupted (see Figs. 10 and 11).

Our classification presented an inspiring capability in extracting intensive aquaculture areas. Fig. 10 showed that almost all those rectangular aquaculture ponds were accurately classified. Whereas a small issue is worth noticing. A few NA pixels nearby the intensive aquaculture ponds were wrongly classified as AA. A possible explanation was that our model was misguided by the dense regular-shaped aquaculture ponds. If these neighboring NA or NW pixels happened to have very similar features compared to AA pixels, it would be likely for our model to incorrectly classify them due to their spatial distribution patterns.

The classification results showed that many AA or NA clusters extracted by our method were slightly bigger than the ground truth. This was partly due to the mixed pixels. It can be seen from Fig. 11 that our model categorized most of the mixed pixels of land cover margins into AA or NA rather than their surrounding NW land types. Fig. 9 showed that the precision of our method on AA was below 85%, and 112 checkpoints labeled NW were wrongly classified as AA. This might be due to the data distribution of sample subimages. In the real world, AA and NA only had a very small proportion compared to NW, from the random checkpoints we can find that NW covered almost 85% of the whole area. However, we took the under-sampling method [42] by dropping many of them to make sure the sample subimages were not way too imbalanced for training a reliable deep learning model. But meanwhile, it also sacrificed some opportunities for our model to fully learn the features of NW areas considering that NW was a complex category rather than a single land cover type. The tradeoff between the data balance and NW distribution pattern in the real world remains a problem and it is worth further exploring.

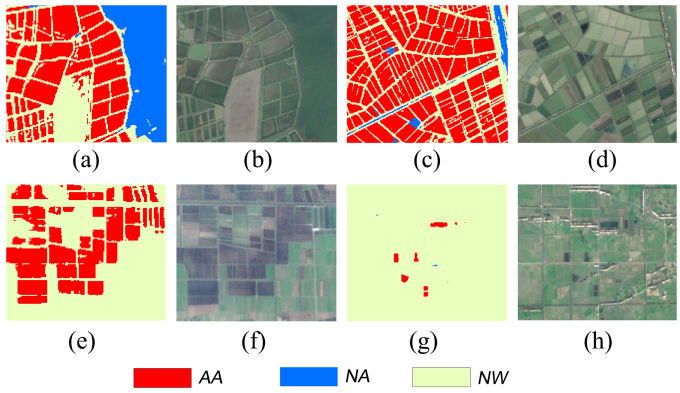

Fig. 15. Classification results on different types of aquaculture areas. (a), (c), (e), and (g) Classification results of enclosure aquaculture areas, intensive aquaculture ponds, integrated rice-crawfish farming areas, and scattered aquaculture ponds, respectively. (b), (d), (f), and (h) Corresponding true color images in order.

We also found that, for different types of aquaculture areas, our classification presented slightly different performances. From Fig. 15, we can see that the classification results on scattered aquaculture ponds were very accurate. Several very small ponds were not recognized and we believed it was limited due to the coarse resolution of raw SAR data. The classification performance on intensive aquaculture ponds was also satisfactory although a few ponds were misclassified to be NW. However, the recognition of integrated rice-crawfish farming areas and enclosure aquaculture areas was found slightly less reliable. Fig. 15(a) and (e) showed that most of these misclassified areas were located in large integral land parcels. We believed that the multiresolution segmentation algorithm split such large-area parcels into several irregular pieces. The object features of all these pieces varied a lot and thus contaminated both the training process and the prediction.

C. Spatial Changes of Aquaculture in Jianghan Plain

The aquaculture maps of different years (see Fig. 12) showed that the aquaculture industry was concentrated in five counties: Hanchuan, Honghu, Jianli, Qianjiang, and Xiantao. The map of 2016 indicated that Hanchuan, Honghu, and Xiantao covered most of the aquaculture areas in Jianghan Plain. It was in accord with the fact that Honghu Lake was the principal freshwater aquaculture area of China [43] and Paihu Lake in Xiantao and Diaochahu Lake in Hanchuan were both important intensive aquaculture farms of Hubei Province.

The aquaculture areas in Qianjiang and Jianli expanded significantly after 2016 (see Figs. 12 and 13) and supported the overall aquaculture areas to reach the top in 2019 (see Fig. 16).

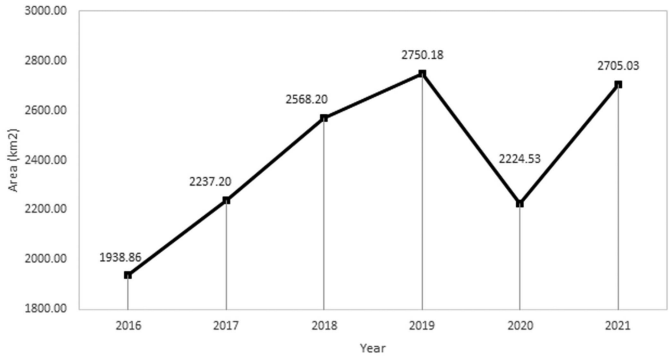

Fig. 16. Area change of the aquaculture industry in Jianghan plain from 2016 to 2021.

An important factor that may have contributed to this change is the rapid growth of IRC farming in recent years [44], [45]. The IRC areas were watered for crawfish breeding before winter.

The sudden descending of the aquaculture area from 2019 to 2020 can be explained by the lockdown of Hubei Province due to the pandemic of Corona Virus Disease 2019 (COVID-19). The decrease in market demand slowed the recovery of the aquaculture industry [46]. The shrinkage of aquaculture areas was majorly driven by the decline of the IRC farming area. Most ponds were fixed but the crawfish breeding was stopped due to the lockdown. This can be verified by Figs. 12 and 13 that the aquaculture areas massively decreased in Qianjiang County while the aquaculture shrinkage in other counties was not that significant. However, the area of the aquaculture industry significantly recovered in 2021. A possible explanation was that the control measures in Hubei Province were loosened and the aquaculture market recovered after the initial stage of panic.

Directly comparing the aquaculture maps of 2016 and 2021, we found some interesting phenomena which can be explained by the policies and social factors in recent years. Most aquaculture areas alongside the lakes such as Honghu Lake and Diaochahu Lake were converted into water and nonwater areas. The enclosure cultures in the lakes and reservoirs in Jianghan Plain were all banned and demolished starting in 2016 for ecosystem recovery [47]. However, the increase of aquaculture areas surrounding the lakes indicated that the enclosure cultures were moved and reformed to aquaculture ponds rather than completely removed. The increase of IRC was possibly an important reason contributing to the significant increase of aquaculture areas in Jianghan Plain (see Fig. 14). Moreover, the Yangtze River fishing ban policies implemented in 2017 and enhanced after Chen et al. [48] have also played a key role in boosting the aquaculture industry by driving the fishery move from wild fishing to aquaculture farming.

The method proposed in this study provided a good result. The classification results were explainable and accorded with the fact. However, it still has shown some potential to be improved. The dynamic maps of aquaculture areas might still be a little deviated from the manually labeled map considering that for each scene and each year we only used one image. Multitemporal images could help increase reliability. For example, the IRC farming fields not watered until late December cannot be distinguished by our method, whereas it still should be counted as the aquaculture area in that year. The parameters of multiscale segmentation used in this study showed good performance in OBIA, however, there still has space to be improved if further research on segmentation method optimization is focused. Besides, the spectral reflectance on the same land object captured by an optical sensor at a different time could be slightly different, which means that our modified UNet cannot achieve full classification capability when applied to images of different years. Some other spectral and object features or even hyperspectral images may be explored in the future to enhance the classification accuracy if possible.

V. Conclusion

In this study, we proposed a novel method using Sentinel-1 and Sentinel-2 data to classify aquaculture areas, nonaquaculture water, and nonwater areas in Jianghan Plain. Image segmentation was applied and multiple indices and features were computed. The optimal 12 datasets were selected by GBDT-based RFE and then imported to our modified UNet for model training. The best classification overall accuracy reached 96.83%. The precision of aquaculture areas reached 84.47% and the recall was 90.48%. The combination of OBIA and PBIA showed its priority compared with other existing classification methods. This method was then applied to the images of the following years for the observation of the spatial distribution and the change in the aquaculture industry in Jianghan Plain. IRC farming was found one of the key factors contributing to the rapid development of aquaculture in recent years. Policies also showed great influences on enclosure culture demolishment for ecosystem restoration and the fishery movement from the Yangtze River to aquaculture farming due to the fishing bans.

References

[1] K. A. Prasad, M. Ottinger, C. Wei, and P. Leinenkugel, "Assessment of coastal aquaculture for India from sentinel-1 SAR time series," *Remote Sens.*, vol. 11, no. 3, 2019, Art. no. 357, doi: 10.3390/rs11030357.

[2] Y. Xu, Z. Hu, Y. Zhang, J. Wang, Y. Yin, and G. Wu, "Mapping aquaculture areas with multi-source spectral and texture features: A case study in the pearl river basin (Guangdong), China," *Remote Sens.*, vol. 13, no. 21, 2021, Art. no. 4320, doi: 10.3390/rs13214320.

[3] X. Hou et al., "Anthropogenic transformation of Yangtze plain freshwater lakes: Patterns, drivers and impacts," *Remote Sens. Environ.*, vol. 248, Oct. 2020, Art. no. 111998, doi: 10.1016/j.rse.2020.111998.

[4] X. Tang, R. Li, D. Han, and M. Scholz, "Response of eutrophication development to variations in nutrients and hydrological regime: A case study in the Changjiang River (Yangtze) basin," *Water*, vol. 12, no. 6, 2020, Art. no. 1634, doi: 10.3390/w12061634.

[5] H. Zhang et al., "Extinction of one of the world's largest freshwater fishes: Lessons for conserving the endangered Yangtze fauna," *Sci. Total Environ.*, vol. 710, Mar. 2020, Art. no. 136242, doi: 10.1016/j.scitotenv.2019.136242.

[6] H. Zhang et al., "Rapid change in Yangtze fisheries and its implications for global freshwater ecosystem management," *Fish Fisheries*, vol. 21, no. 3, pp. 601–620, 2020, doi: 10.1111/faf.12449.

[7] L. Cao et al., "Environmental impact of aquaculture and countermeasures to aquaculture pollution in China," *Environ. Sci. Pollut. Res. Int.*, vol. 14, no. 7, pp. 452–462, Nov. 2007, doi: 10.1065/espr2007.05.426.

[8] S. Xia et al., "Restriction of herbivorous waterbird distributions in the middle and lower Yangtze River floodplain in view of hydrological isolation," *Wetlands*, vol. 37, no. 1, pp. 79–88, Feb. 2017, doi: 10.1007/s13157-016-0841-9.

[9] Y. Dai et al., "Policy-driven changes in enclosure fisheries of large lakes in the Yangtze Plain: Evidence from satellite imagery," *Sci. Total Environ.*, vol. 688, pp. 1286–1297, Oct. 2019, doi: 10.1016/j.scitotenv.2019.06.179.

[10] Z. Jiang and Y. Ma, "Accurate extraction of offshore raft aquaculture areas based on a 3D-CNN model," *Int. J. Remote Sens.*, vol. 41, no. 14, pp. 5457–5481, Jul. 2020, doi: 10.1080/01431161.2020.1737340.

[11] Y. Duan et al., "Tracking changes in aquaculture ponds on the China coast using 30 years of Landsat images," *Int. J. Appl. Earth Observ. Geoinf.*, vol. 102, Oct. 2021, Art. no. 102383, doi: 10.1016/j.jag.2021.102383.

[12] M. Ottinger, K. Clauss, and C. Kuenzer, "Large-scale assessment of coastal aquaculture ponds with sentinel-1 time series data," *Remote Sens.*, vol. 9, no. 5, 2017, Art. no. 440, doi: 10.3390/rs9050440.

[13] Z. Sun et al., "Nation-scale mapping of coastal aquaculture ponds with sentinel-1 SAR data using google earth engine," *Remote Sens.*, vol. 12, no. 18, 2020, Art. no. 3086, doi: 10.3390/rs12183086.

[14] Y. Fu et al., "Finer resolution mapping of marine aquaculture areas using worldview-2 imagery and a hierarchical cascade convolutional neural network," *Remote Sens.*, vol. 11, no. 14, 2019, Art. no. 1678, doi: 10.3390/rs11141678.

[15] B.-G. Cui et al., "Floating raft aquaculture area automatic extraction based on fully convolutional network," *J. Coastal Res.*, vol. 90, no. SI, pp. 86–94, 2019, doi: 10.2112/si90-011.1.

[16] M. Wang, Q. Cui, J. Wang, D. Ming, and G. Lv, "Raft cultivation area extraction from high resolution remote sensing imagery by fusing multi-scale region-line primitive association features," *ISPRS J. Photogram. Remote Sens.*, vol. 123, pp. 104–113, Jan. 2017, doi: 10.1016/j.isprsjprs.2016.10.008.

[17] C. Ren et al., "Rapid expansion of coastal aquaculture ponds in China from Landsat observations during 1984–2016," *Int. J. Appl. Earth Observ. Geoinf.*, vol. 82, Oct. 2019, Art. no. 101902, doi: 10.1016/j.jag.2019.101902.

[18] Y. Liu et al., "Satellite-based monitoring and statistics for raft and cage aquaculture in China's offshore waters," *Int. J. Appl. Earth Observ. Geoinf.*, vol. 91, Sep. 2020, Art. no. 102118, doi: 10.1016/j.jag.2020.102118.

[19] Z. Zeng, D. Wang, W. Tan, and J. Huang, "Extracting aquaculture ponds from natural water surfaces around inland lakes on medium resolution multispectral images," *Int. J. Appl. Earth Observ. Geoinf.*, vol. 80, pp. 13–25, Aug. 2019, doi: 10.1016/j.jag.2019.03.019.

[20] Y. Gan, K. Zhao, Y. Deng, X. Liang, T. Ma, and Y. Wang, "Groundwater flow and hydrogeochemical evolution in the Jianghan plain, central China," *Hydrogeol. J.*, vol. 26, no. 5, pp. 1609–1623, Aug. 2018, doi: 10.1007/s10040-018-1778-2.

[21] F. Filipponi, "Sentinel-1 GRD preprocessing workflow," *Proceedings*, vol. 18, no. 1, 2019, Art. no. 11, doi: 10.3390/ECRS-3-06201.

[22] M. Main-Knorn, B. Pflug, J. Louis, V. Debaecker, U. Müller-Wilm, and F. Gascon, "Sen2Cor for sentinel-2," *Proc. SPIE*, 2017, Art. no. 10427, doi: 10.1117/12.2278218.

[23] Y. Du, Y. Zhang, F. Ling, Q. Wang, W. Li, and X. Li, "Water bodies' mapping from sentinel-2 imagery with modified normalized difference water index at 10-m spatial resolution produced by sharpening the SWIR band," *Remote Sens.*, vol. 8, no. 4, 2016, Art. no. 354, doi: 10.3390/rs8040354.

[24] Z. Wang, J. Liu, J. Li, and D. D. Zhang, "Multi-spectral water index (MuWI): A native 10-m multi-spectral water index for accurate water mapping on sentinel-2," *Remote Sens.*, vol. 10, no. 10, 2018, Art. no. 1643, doi: 10.3390/rs10101643.

[25] B. Du et al., "Mapping wetland plant communities using unmanned aerial vehicle hyperspectral imagery by comparing object/pixel-based classifications combining multiple machine-learning algorithms," *IEEE J. Sel. Topics Appl. Earth Observ. Remote Sens.*, vol. 14, pp. 8249–8258, 2021, doi: 10.1109/JSTARS.2021.3100923.

[26] Y. Han, Z. Liu, K. Khoshelham, and S. H. Bai, "Quality estimation of nuts using deep learning classification of hyperspectral imagery," *Comput. Electron. Agriculture*, vol. 180, Jan. 2021, Art. no. 105868, doi: 10.1016/j.compag.2020.105868.

[27] U. C. Benz, P. Hofmann, G. Willhauck, I. Lingenfelder, and M. Heynen, "Multi-resolution, object-oriented fuzzy analysis of remote sensing data for GIS-ready information," *ISPRS J. Photogram. Remote Sens.*, vol. 58, no. 3, pp. 239–258, Jan. 2004, doi: 10.1016/j.isprsjprs.2003.10.002.

[28] S. Jabari and Y. Zhang, "Very high resolution satellite image classification using fuzzy rule-based systems," *Algorithms*, vol. 6, no. 4, pp. 762–781, 2013, doi: 10.3390/a6040762.

[29] L. Jiao, W. Sun, G. Yang, G. Ren, and Y. Liu, "A hierarchical classification framework of satellite multispectral/hyperspectral images for mapping coastal wetlands," *Remote Sens.*, vol. 11, no. 19, 2019, Art. no. 2238, doi: 10.3390/rs11192238.

[30] Z. Xia, X. Guo, and R. Chen, "Automatic extraction of aquaculture ponds based on Google Earth engine," *Ocean Coast Manage.*, vol. 198, Dec. 2020, Art. no. 105348, doi: 10.1016/j.ocecoaman.2020.105348.

[31] J. Su, D. Yi, C. Liu, L. Guo, and W.-H. Chen, "Dimension reduction aided hyperspectral image classification with a small-sized training dataset: Experimental comparisons," *Sensors,* vol. 17, no. 12, 2017, Art. no. 2726, doi: 10.3390/s17122726.

[32] I. Guyon, J. Weston, S. Barnhill, and V. Vapnik, "Gene selection for cancer classification using support vector machines," *Mach. Learn.*, vol. 46, no. 1, pp. 389–422, Jan. 2002, doi: 10.1023/A:1012487302797.

[33] L. Yang, L. R. Mansaray, J. Huang, and L. Wang, "Optimal segmentation scale parameter, feature subset and classification algorithm for geographic object-based crop recognition using multisource satellite imagery," *Remote Sens.*, vol. 11, no. 5, 2019, Art. no. 514, doi: 10.3390/rs11050514.

[34] Y. Han et al., "Impact analysis of environmental and social factors on early-stage COVID-19 transmission in China by machine learning," *Environ Res.*, vol. 208, May 2022, Art. no. 112761, doi: 10.1016/j.envres.2022.112761.

[35] Y. Qi, "Random forest for bioinformatics," in *Ensemble Machine Learning: Methods and Applications*, C. Zhang and Y. Ma, Eds. Berlin, Germany: Springer, 2012, pp. 307–323, doi: 10.1007/978-1-4419-9326-7_11.

[36] B. Neupane, T. Horanont, and J. Aryal, "Deep learning-based semantic segmentation of urban features in satellite images: A review and meta-analysis," *Remote Sens.*, vol. 13, no. 4, 2021, Art. no. 808, doi: 10.3390/rs13040808.

[37] L. Garg, P. Shukla, S. Singh, V. Bajpai, and U. Yadav, "Land use land cover classification from satellite imagery using mUnet: A modified unet architecture," in *Proc. 14th Int. Conf. Comput. Vis. Theory Appl.*, 2019, pp. 359–365, doi: 10.5220/0007370603590365.

[38] J. McGlinchy, B. Johnson, B. Muller, M. Joseph, and J. Diaz, "Application of UNet fully convolutional neural network to impervious surface segmentation in urban environment from high resolution satellite imagery," in *Proc. IEEE Int. Geosci. Remote Sens. Symp.*, 2019, pp. 3915–3918, doi: 10.1109/IGARSS.2019.8900453.

[39] O. Ronneberger, P. Fischer, and T. Brox, "U-Net: Convolutional networks for biomedical image segmentation," in *Proc. Int. Conf. Med. Image Comput. Comput.-Assist. Intervention*, 2015, pp. 234–241, doi: 10.1007/978-3-319-24574-4_28.

[40] Y. Duan, X. Li, L. Zhang, D. Chen, S. A. Liu, and H. Ji, "Mapping national-scale aquaculture ponds based on the Google Earth engine in the Chinese coastal zone," *Aquaculture,* vol. 520, Apr. 2020, Art. no. 734666, doi: 10.1016/j.aquaculture.2019.734666.

[41] T. Kattenborn, J. Leitloff, F. Schiefer, and S. Hinz, "Review on convolutional neural networks (CNN) in vegetation remote sensing," *ISPRS J. Photogram. Remote Sens.*, vol. 173, pp. 24–49, Mar. 2021, doi: 10.1016/j.isprsjprs.2020.12.010.

[42] A. Fernández, S. del Río, N. V. Chawla, and F. Herrera, "An insight into imbalanced big data classification: Outcomes and challenges," *Complex Intell. Syst.*, vol. 3, no. 2, pp. 105–120, Jun. 2017, doi: 10.1007/s40747-017-0037-9.

[43] X. Xiong, Q. Liu, X. Chen, R. Wang, M. Duan, and C. Wu, "Occurrence of microplastic in the water of different types of aquaculture ponds in an important lakeside freshwater aquaculture area of China," *Chemosphere,* vol. 282, Nov. 2021, Art. no. 131126, doi: 10.1016/j.chemosphere.2021.131126.

[44] Y. Chen, P. Yu, Y. Chen, and Z. Chen, "Spatiotemporal dynamics of rice–crayfish field in mid-China and its socioeconomic benefits on rural revitalisation," *Appl. Geogr.*, vol. 139, Feb. 2022, Art. no. 102636, doi: 10.1016/j.apgeog.2022.102636.

[45] Y. Wei, M. Lu, Q. Yu, A. Xie, Q. Hu, and W. Wu, "Understanding the dynamics of integrated rice–crawfish farming in Qianjiang county, China using Landsat time series images," *Agricultural Syst.*, vol. 191, Jun. 2021, Art. no. 103167, doi: 10.1016/j.agsy.2021.103167.

[46] G. M. M. Alam, M. N. I. Sarker, M. Gatto, H. Bhandari, and D. Naziri, "Impacts of COVID-19 on the fisheries and aquaculture sector in developing countries and ways forward," *Sustainability,* vol. 14, no. 3, 2022, Art. no. 1071, doi: 10.3390/su14031071.

[47] Hubei Provincial Department of Agriculture and Hubei Provincial Department of Water Resources. *Notice on regulating the breeding behavior of lakes and reservoirs*. 2016. [Online]. Available: https://sft.hubei.gov.cn/bsfw/bmcxfw/gfxwjcxxt/202102/t20210203_3333531.shtml

[48] T. Chen, Y. Wang, C. Gardner, and F. Wu, "Threats and protection policies of the aquatic biodiversity in the Yangtze River," *J. Nature Conservation*, vol. 58, Dec. 2020, Art. no. 125931, doi: 10.1016/j.jnc.2020.125931.

Yifei Han received the B.S. degree in remote sensing science and technology from the Wuhan University, Wuhan, China, in 2006, and the M.S. degree in spatial engineering from the University of Melbourne, Parkville, VIC, Australia, in 2020. He is currently working toward the Ph.D. degree in physical geography with the Key Laboratory of Monitoring and Estimate for Environment and Disaster of Hubei Province, Innovation Academy for Precision Measurement Science and Technology, Chinese Academy of Sciences, Beijing, China.

His research interests include super-resolution of remote sensing images and land cover mapping.

Jinliang Huang received the B.S. degree in geomorphology from the Beijing University, Beijing, China, in 1988, and the M.S. degree in physical geography from the State Key Laboratory of Resources and Environmental Information System (LREIS), Institute of Geographical Sciences and Natural Resources Research, Chinese Academy of Sciences, Beijing, China, in 1996, and Ph.D. degree in historical physical geography from the Wuhan University, Wuhan, China, in 2002.

He is currently a Professor with the Innovation Academy for Precision Measurement Science and Technology, Chinese Academy of Sciences. He has also been a visiting scholar with the University of Liverpool, Liverpool, U.K., and the University College of London, London, U.K., both in 2000. His research interests include application of remote sensing and geographic information system, land use and regional sustainable development, ecological environment, and environmental change.

Feng Ling received the B.S. degree in geology and the M.S. degree in geophysical prospecting and information technology from the China University of Geosciences, Wuhan, China, in 1999 and 2002, respectively, and the Ph.D. degree in system analysis and integration from the Huazhong University of Science and Technology, Wuhan, China, in 2006.

He is currently a professor with the Innovation Academy for Precision Measurement Science and Technology, Chinese Academy of Sciences. He has also been a visiting scholar with the University of Nottingham, Nottingham, U.K., in 2016. He has authored or coauthored more than 100 refereed journal articles. His research interests include super-resolution land cover mapping, spatial-temporal fusion of remotely sensed imagery, and water resources monitoring.

Dr. Ling is currently an Associate Editor for *Remote Sensing in Ecology and Conservation* and *Remote Sensing Letters*. He is the recipient of the 2016 Boeing Award for Best Scientific Paper in Image Analysis and Interpretation from the American Society for Photogrammetry and Remote Sensing and the 2020 Taylor and Francis Remote Sensing Letters Award.

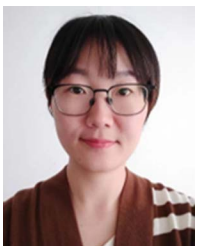

Juan Qiu received the B.S. degree in geographical science from the Hubei University, Wuhan, China, in 2008, and the Ph.D. degree in physical geography from the Institute of Geodesy and Geophysics, Chinese Academy of Sciences,Wuhan, China, in 2014.

She is currently a Research Associate with the Innovation Academy for Precision Measurement Science and Technology, Chinese Academy of Sciences. Her research interest include land cover mapping by remotely sensed imagery.

Zhixuan Liu received the B.S. degree in geographic information science from the Hubei University, Wuhan, China, in 2023. She is currently working toward the M.S. degree in surveying and mapping with the China University of Mining and Technology, Beijing, China.

Her research interests include surveying and mapping technology and the application of geographic information system.

Xiaodong Li received the B.S. degree in geographic information system from the China University of Geosciences,Wuhan, China, in 2006, and the M.S. and Ph.D. degrees in physical geography from the Institute of Geodesy and Geophysics, Chinese Academy of Sciences,Wuhan, China, in 2009 and 2012, respectively.

He is currently a Professor with the Innovation Academy for Precision Measurement Science and Technology, Chinese Academy of Sciences. He has been supported by the Youth Innovation Promotion Association, CAS, and the Hubei Province Natural Science Fund for Distinguished Young Scholars. His research interest include super-resolution mapping of remotely sensed imagery.

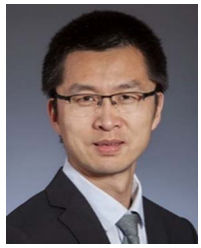

Cun Chang received the B.S. in geography from the Xinjiang University, Urumqi, China, in 2004, and the Ph.D. degree in cartography and geographic information systems from the Graduate University of Chinese Academy of Sciences, Beijing, China, in 2010.

He is currently a Senior Engineer with the State Key Laboratory of Desert and Oasis Ecology, Xinjiang Institute of Ecology and Geography, Chinese Academy of Sciences, Urumqi, China. His research interests include remote sensing interpretation of land cover in arid areas and geospatial data mining and analysis.

Hong Chi received the B.S. degree in information engineering from the Wuhan University, Wuhan, China, and the M.S. degree in cartography and geographic information systems from the Fuzhou University, Fuzhou, China, in 2003 and 2008, respectively, and the Ph.D. degree in cartography and geographic information systems from the Aerospace Information Research Institute, Chinese Academy of Sciences, Beijing, China, in 2011.

He is currently an Associate Professor with the Innovation Academy for Precision Measurement Science and Technology, Chinese Academy of Sciences, Wuhan, China. His research interests include land cover mapping, vegetation remote sensing, ecological parameter inversion, and simulation from remotely sensed imagery.